Applied Surface Science xxx (2016) xxx–xxx

Contents lists available at ScienceDirect

Applied Surface Science

journal homepage: www.elsevier.com/locate/apsusc

Full Length Article

Spectroscopic ellipsometry characterization of ZnO:Sn thin films with various Sn composition deposited by remote-plasma reactive sputtering

Petr Janicek[a,b,*], Kham M. Niang[c], Jan Mistrik[a,b], Karel Palka[d,b], Andrew J. Flewitt[c]

[a] Faculty of Chemical Technology, Institute of Applied Physics and Mathematics, University of Pardubice, Studentska 95, 53210 Pardubice, Czechia
[b] Faculty of Chemical Technology, Center of Materials and Nanotechnologies, University of Pardubice, nam. Cs. legii 565, 530 02 Pardubice, Czechia
[c] Electrical Engineering Division, Cambridge University, 9 J J Thomson Avenue, Cambridge CB3 0FA, UK
[d] Faculty of Chemical Technology, Department of General and Inorganic Chemistry, University of Pardubice, Studentska 95, 53210 Pardubice, Czechia

ARTICLE INFO

Article history:
Received 29 July 2016
Received in revised form 19 October 2016
Accepted 25 October 2016
Available online xxx

Keywords:
Spectroscopic ellipsometry
Remote-plasma reactive sputtering
ZnO:Sn
Optical properties

ABSTRACT

ZnO:Sn thin films were deposited onto thermally oxidized silicon substrates using a remote plasma reactive sputtering. Their optical constants (refractive index n and extinction coefficient k) were determined from ellipsometric data recorded over a wide spectral range (0.05–6 eV). Parametrization of ZnO:Sn complex dielectric permittivity consists of a parameterized semiconductor oscillator function describing the short wavelength absorption edge, a Drude oscillator describing free carrier absorption in near-infrared part of spectra and a Lorentz oscillator describing the long wavelength absorption edge and intra-band absorption in the ultra-violet part of the spectra. Using a Mott-Davis model, the increase in local disorder with increasing Sn doping is quantified from the short wavelength absorption edge onset. Using the Wemple-DiDomenico single oscillator model for the transparent part of the optical constants spectra, an increase in the centroid distance of the valence and conduction bands with increasing Sn doping is shown and only slight increase in intensity of the inter-band optical transition due to Sn doping occurs. The Drude model applied in the near-infrared part of the spectra revealed the free carrier concentration and mobility of ZnO:Sn. Results show that the range of transparency of prepared ZnO:Sn layers is not dramatically affected by Sn doping whereas electrical conductivity could be controlled by Sn doping. Refractive index in the transparent part is comparable with amorphous Indium Gallium Zinc Oxide allowing utilization of prepared ZnO:Sn layers as an indium-free alternative.

© 2016 The Authors. Published by Elsevier B.V. This is an open access article under the CC BY license (http://creativecommons.org/licenses/by/4.0/).

1. Introduction

Transparent conductive oxides (TCOs), which are derived from wide band-gap semiconductors with low resistivity and high transparency in the visible spectrum, have been used in flat panel displays for many decades. The most widely used material is indium tin oxide (ITO) [1]. However, due to the concerns over the shortage of supply and high cost of indium, aluminium- or gallium- doped zinc oxides (AZO or GZO) have been intensively investigated as alternatives to ITO. Both the electrical and optical properties of these materials have been reported. In particular, spectroscopic ellipsometry has been widely used to investigate the dielectric functions of ZnO in a broad spectral range [2–6].

Amorphous oxide semiconductors (AOSs) such as doped ZnO are also used as channel layers in thin film transistors (TFTs). The requirement for this is different from TCOs. A resistive film with a well-controlled carrier concentration, high carrier mobility and preferably amorphous microstructure for better uniformity over large area are required. Various multi-component AOSs have been incorporated in TFTs [7], and the leading material, amorphous indium gallium zinc oxide (a-IGZO) has been demonstrated in displays [8]. Amorphous zinc tin oxide (a-ZTO) is an important indium-free alternative to the a-IGZO, and TFTs incorporating this material show high carrier mobility [9]. While the electrical properties of these materials have been well investigated, there are fewer reports on their optical properties [10–12].

Ellipsometric studies on high quality, single crystalline ZnO that have been epitaxially grown on sapphire substrates have shown

* Corresponding author at: Faculty of Chemical Technology, Institute of Applied Physics and Mathematics, University of Pardubice, Studentska 95, 53210 Pardubice, Czechia.
E-mail address: petr.janicek@upce.cz (P. Janicek).

http://dx.doi.org/10.1016/j.apsusc.2016.10.169
0169-4332/© 2016 The Authors. Published by Elsevier B.V. This is an open access article under the CC BY license (http://creativecommons.org/licenses/by/4.0/).

Please cite this article in press as: P. Janicek, et al., Spectroscopic ellipsometry characterization of ZnO:Sn thin films with various Sn composition deposited by remote-plasma reactive sputtering, Appl. Surf. Sci. (2016), http://dx.doi.org/10.1016/j.apsusc.2016.10.169

that the band edge transition occurs at 3.3 eV [5] and that the surface roughness needs to be accounted for to achieve the best fitting of the measured data [3]. A shift in the absorption edge has also been reported when ZnO is doped with either aluminum or gallium in TCOs [4]. Similarly, AZO deposited by direct current magnetron sputtering shows an increase in the optical bandgap with the efficiency of aluminum doping in the film [13]. A Tauc-Lorentz model with a Lorentz-type oscillator is applied on the optical absorption spectra of crystalline (c-IGZO) and a-IGZO, which is further divided into high or low quality films depending on their Hall mobilities [10]. While an optical transition ~3.7 eV is determined for all the films, significant differences in the dielectric functions are observed which are attributed to the cation content, the crystallinity and the quality of the films [10].

In this paper, spectroscopic ellipsometry was used to study the optical properties of ZnO:Sn with various tin doping produced by remote-plasma reactive sputtering. The effect of tin doping on the complex dielectric functions of the ZTO are investigated over a broad spectral range from 0.05 to 6 eV. In the vicinity of the absorption edge ($3.0 < E < 4.0$ eV) a Mott-Davis model, in the semi-transparent spectrum ($0.5 < E < 2.5$ eV) a Wemple-DiDomenico single oscillator dispersion, and in the mid-infra-red (MIR) ($0.2 < E < 0.5$ eV) a Drude model were employed as this analysis provide physical meaning of the extracted parameters.

2. Experimental details

ZnO:Sn thin films were deposited onto thermally oxidized silicon substrates using a remote plasma reactive sputtering without intentional substrate heating. Zinc: tin metal alloy targets with tin compositions of 10, 33 and 50 atomic% were used. For reference, undoped ZnO were also deposited from a 100% zinc targets using the same sputtering conditions. The details of the system and the deposition conditions can be found elsewhere [14], and are simply summarized here. Films were deposited for times between 10 and 15 min with an optimized flow of argon and oxygen (60 sccm and 35 sccm respectively) at a pressure $\sim 6 \times 10^{-3}$ mbar during sputtering. The deposited films were highly resistive which are suitable as channel layers in TFTs [14]. Moreover, it has been confirmed that the as-deposited ZnO:Sn thin films are amorphous while the as-deposited ZnO thin film is polycrystalline [14].

Chemical compositions were determined using energy dispersive X-ray spectroscopy (EDS) (Aztec X-Max 20, Oxford Instruments) attached to the scanning electron microscope (LYRA 3, Tescan) where each sample was analyzed at two spots ($100 \times 100\,\mu$m size) and the data were averaged. The ratio of tin compositions in the ZnO:Sn films were determined to be ~33, 50 and 65 atomic%. Therefore, the undoped ZnO and doped ZnO samples are denoted as ZT0, ZT33, ZT50 and ZT65. No post-deposition annealing had been performed. Surface topography was also studied using atomic force microscopy (Solver NEXT, NT-MDT). Two measurements (spot size $10 \times 10\,\mu$m) were performed on each sample and the average root mean square (RMS) of the surface roughness was determined according to the ISO 4287/1.

Optical characterizations were performed using two variable angle spectroscopic ellipsometers (VASE and IR-VASE, J. A. Woollam Co.). The first, rotating analyzer ellipsometer, operates in the spectral range 190 nm–1700 nm (ultra-violet (UV)–vis (VIS)-near-infrared (NIR)). Measurements with 30 analyzer revolutions with photon energy steps of 0.05 eV at three selected angles of incidence (AOI) at 50°, 60° and 70° were performed for each sample. The second, rotating compensator ellipsometer, covers the spectral range 1.7 µm–22 µm (NIR-MIR). Spectra for AOI of 50°, 60° and 70° were recorded (measuring 25 scans, 15 spectra per revolution, with wavenumber steps 8 cm^{-1}). Near normal incidence optical reflectance was measured by the same instruments. WVASE32 software was used for modeling of the measured data.

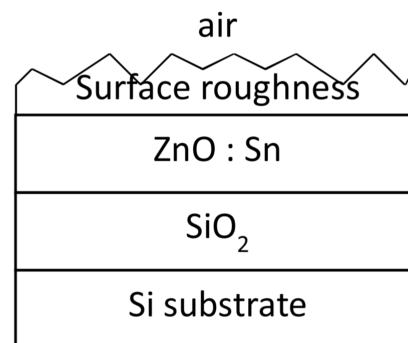

Fig. 1. Sketch of the optical model used to fit the ellipsometry data.

3. Results and discussion

3.1. Structure model and material optical constants

As shown in Fig. 1, a sample model used to analyze the raw ellipsometry data consists of i) a semi-infinite crystalline silicon substrate, ii) a SiO_2 layer, iii) a homogenous, isotropic layer representing the ZnO:Sn layer, iv) surface roughness and v) air as the ambient medium.

Optical constants of Si and SiO_2 in the NIR-VIS-UV ranges were taken from the literature [15]. Optical constants of Si and SiO_2 layer in the MIR part of spectra was obtained by measurement of an uncoated SiO_2/Si substrate.

In the literature different models describing mostly the transparent part of the spectra for ZnO, such as Cauchy or Sellmeier have been reported [16]. Mammadov et al. have applied the parameterized semiconductor oscillator function (PSEMI) model for describing the dielectric function of ZnO over a wide spectral range [6]. The PSEMI model analytically describes the dielectric functions as the summation of several energy-bounded Gaussian-broadened polynomials and poles accounting for index effects due to absorption occurring outside the region being modeled [17–19].

In this work, the model dielectric function used for the ZnO:Sn layer consists of several contributions:

$$\tilde{\varepsilon} = \tilde{\varepsilon}_{PSEMI} + \sum \tilde{\varepsilon}_{Lorentz} + \tilde{\varepsilon}_{Drude} \quad (1)$$

The above mentioned PSEMI oscillator functions sufficiently describes the short wavelength absorption edge of amorphous doped ZnO:Sn samples and polycrystalline undoped ZnO samples as well. In addition, a Lorentz oscillator is further applied to model inter band transitions in the UV [20]. In the MIR region ($0.05 < E < 0.5$ eV), Lorentz oscillator functions are used to model the long wavelength absorption edge and a Drude oscillator to model free carrier absorption [21]. Surface roughness is modeled by a Bruggeman type effective medium approximation [22] with 50% of voids and 50% of ZnO:Sn.

3.2. Figure of merit and quality of the fit

The measured spectroscopic ellipsometry parameters, ψ^{exp} and Δ^{exp}, are fitted against the designed model in the spectral range

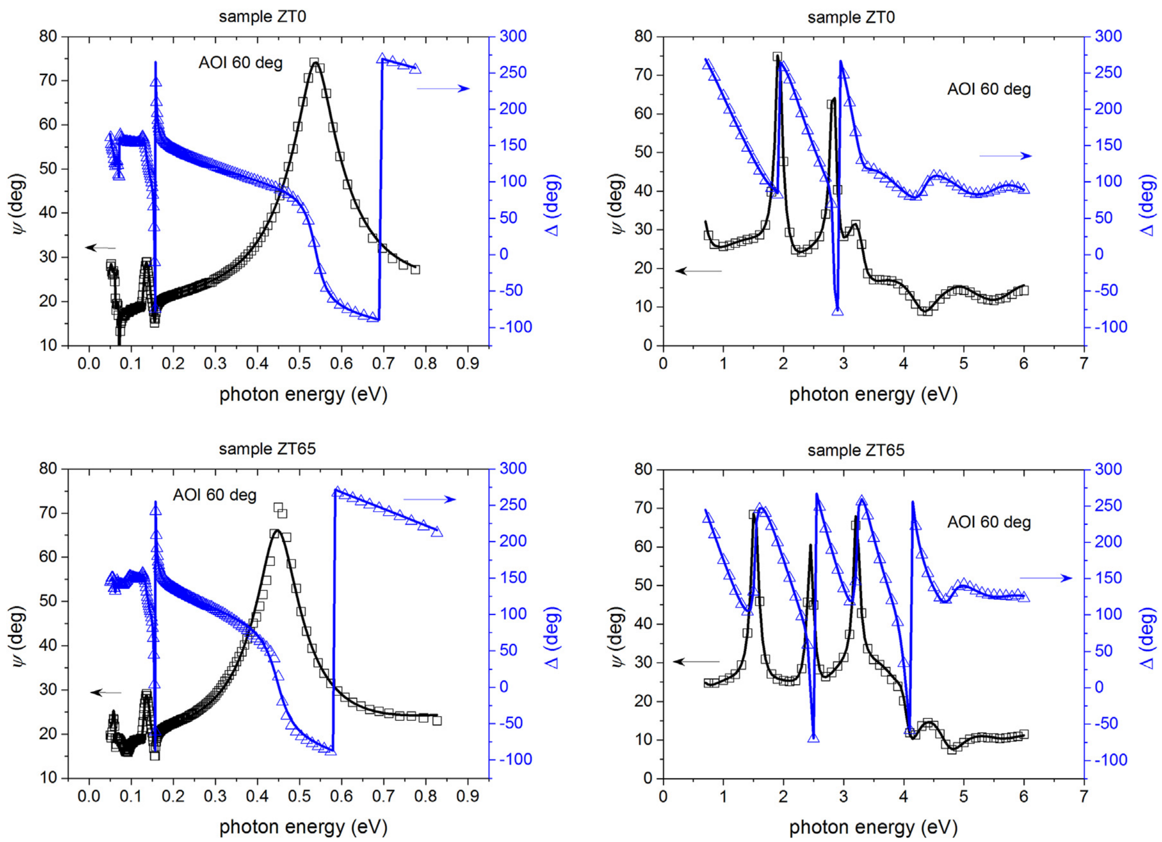

Fig. 2. Measured values of ψ (circles) and Δ (triangles) for samples ZT0 and ZT65 in the MIR part of the spectrum (left column) and NIR-VIS-UV part of the spectra (right column). The best fit for the angle of incidence 60° is shown by solid lines.

from 0.05 eV to 6 eV using the mean square error (MSE) given in the following expression:

$$MSE = \sqrt{\frac{1}{2N-M}\sum_{i=1}^{N}\left[\left(\frac{\psi_i^{mod}-\psi_i^{exp}}{\sigma_{\psi,i}^{exp}}\right)^2+\left(\frac{\Delta_i^{mod}-\Delta_i^{exp}}{\sigma_{\Delta,i}^{exp}}\right)^2\right]} \quad (2)$$

where N is the number of measured pairs of ellipsometric parameters ψ^{exp} and Δ^{exp} and M represents the total number of fitted parameters. $\sigma_{\psi,i}^{exp}$ and $\sigma_{\Delta,i}^{exp}$ are then the estimated experimental error of ψ^{exp} and Δ^{exp}, respectively. Ellipsometric data measured for all three angles of incidence 50°, 60° and 70° were used in the fit simultaneously.

Fig. 2 shows the spectra of the ellipsometry parameters, ψ (circles) and Δ (triangles) for an AOI of 60° in the spectral range from 0.05 to 0.8 eV (MIR part of spectrum, left column) and from 0.9 to 6 eV (NIR-VIS-UV part of spectrum, right column). Two samples, ZT0 and ZT65 are chosen to represent the polycrystalline ZnO and amorphous ZT layers respectively. Good agreement (MSE less than 5) was obtained between the measured (symbols) and calculated data (solid lines) for both ZT0 and ZT65.

3.3. Film thickness and surface roughness

Measurement of the uncoated SiO_2/Si substrate revealed a SiO_2 layer thickness of 216 nm. In all models used for evaluation of ellipsometry data, the thickness of the SiO_2 was not fixed but was used as one of the free parameters. Measured thicknesses of SiO_2 and ZT films are summarized in Table 1 together with the MSE values calculated in the range from 0.05 eV to 6 eV.

Fig. 3 compares the surface roughness determined by ellipsometry with AFM measurements. Ellipsometry data shows that the

Table 1
Thickness of SiO_2 and ZT films obtained by the best fit of ellipsometry data together with MSE values.

Sample	Thickness SiO_2 (nm)	ZT film thickness (nm)	MSE
Un-deposited (reference)	216.0 ± 0.2	N.A.	2.3
ZT0	207.5 ± 0.2	143.9 ± 0.2	3.0
ZT33	208.4 ± 0.2	228.4 ± 0.2	3.3
ZT50	203.2 ± 0.2	291.5 ± 0.5	4.3
ZT65	206.1 ± 0.2	226.2 ± 0.3	5.3

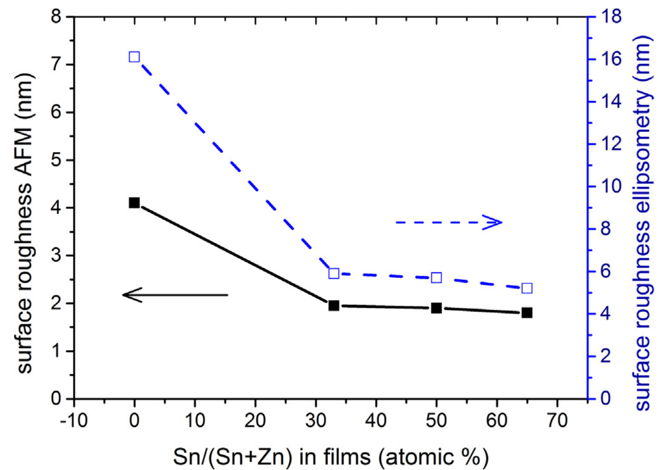

Fig. 3. Comparison of surface roughness determined by SE (dashed line) and AFM (solid lines) as a function of tin doping in the ZT films.

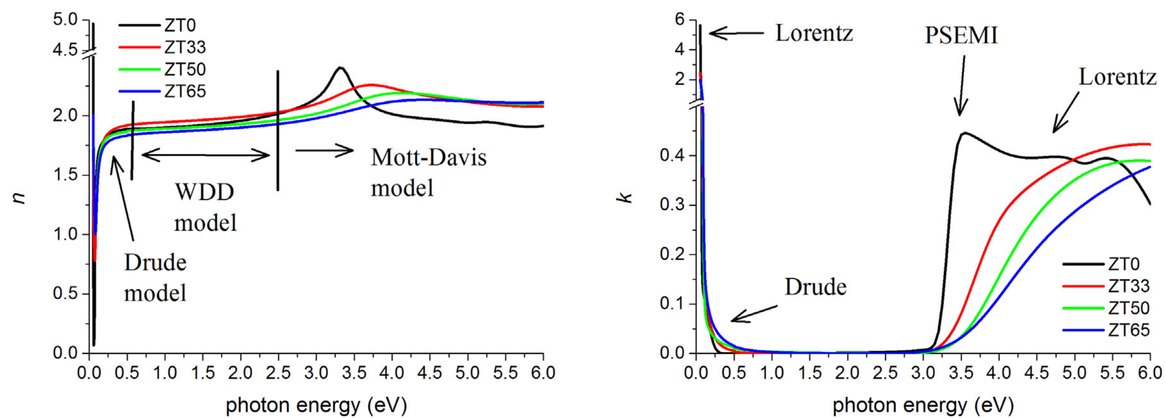

Fig. 4. Determined ZT refractive index *n*, and extinction coefficient *k*, as a function of photon energy in the wide spectral range. Indication of spectral ranges where different models (Mott-Davis, Wemple-DiDomenico (WDD) and Drude) are used (left), indicate the different oscillators used (right). Note that Drude oscillator has not been used for ZT0 sample.

surface roughness of ZT0 is ~16 nm and that it decreases sharply to ~6 nm in ZT33, 50 and 65. A similar trend of decreasing surface roughness with increase in tin doping is observed in AFM data. The difference in the values obtained by the two techniques can be rationalized if we consider the distinctive nature of the SE and AFM measurements: SE roughness is a mixture of material and voids, while AFM "physically" measures the average height of the features on top of the film bulk [23–25]. The surface roughness of ZnO:Sn films are generally smaller than undoped ZnO film. This can be attributed to their amorphous nature, in contrast with the polycrystalline nature of undoped ZnO film [14]. The surface roughnesses among the Sn doped ZT layers are very similar (within the experimental error).

3.4. Refractive index and extinction coefficients of ZnO:Sn in wide spectral range

Fig. 4 shows determined wide spectral range dispersion of the refractive index, *n*, and extinction coefficient, *k*, of ZT films. In the NIR-VIS-UV region ($0.5 < E < 6.0$ eV), undoped ZT0 shows a narrow profile of refractive index with a peak at ~3.2 eV. On the contrary, the doped samples (ZT33 to ZT65) show broader profiles with peaks at higher energies than the undoped sample. Moreover, the intensities (heights) of the peaks are also lower. Comparing among the doped samples (ZT33, ZT50 and ZT65), it is observed that the peak energy shifts to higher energy and the profile gets broader (with the corresponding decrease in intensity) with increased doping concentration.

The refractive index and extinction coefficient of ZT0 here is consistent with reported crystalline ZnO films grown epitaxially by pulsed laser deposition or by sputtering [5,26]. The refractive index decreases with increase in tin doping in the broad range of 0.5–4 eV, which is consistent with an increase in carrier concentration due to incorporation of Sn ions (with valency +3 or +4) in the ZnO [4,27,28].

The extinction coefficient of the undoped ZT0 rises sharply at ~3.2 eV and those of doped ZT samples rise comparatively slowly. This difference can also be attributed to the polycrystalline and amorphous nature of the undoped and doped ZT samples respectively. The extinction coefficient of both the undoped and doped sample is ~0 in the visible spectrum which is typical of wide band gap TCO and AOS materials.

In the MIR region ($0.05 < E < 0.5$ eV), typical phonon modes of ZnO (undoped ZT0) are present which result in high *k* values [29,6]. ZT0 sample has been fitted by harmonic oscillator approximation without Drude oscillator with the results of ZT0 here is consistent with reported crystalline ZnO films deposited by magnetron sputtering or by pulsed laser deposition [29]. On the contrary, the doped samples (ZT33 to ZT65) show broader profiles with peaks at higher energies than the undoped sample. Moreover, the intensities (heights) of the peaks are also lower consistently within the NIR-VIS-UV region.

Finally, as shown in Fig. 4, in semi-transparent part of spectra the extinction coefficient, *k*, is very small (ideally zero). Therefore, the real part of the complex refractive index, *n*, has been used to gauge the quality of the films for use in electronic devices. A refractive index ~2 is obtained for both undoped and doped ZT samples; this is similar to that reported for a-IGZO [10–12]. A high value of refractive index indicates a low void concentration in the film, which is desirable [30].

It is worth to mention that Tauc-Lorentz oscillator [31,32] which is usually used for description of short wavelength edge of amorphous semiconductors could be also successfully used instead of PSEMI oscillator in the case of ZT33, ZT50 and ZT65 samples leading us to the idea that these samples exhibit indirect optical band gap. On the contrary Tauc-Lorentz oscillator cannot usefully describe direct optical band gap of ZT0 sample. Results obtained by Tauc-Lorentz oscillator will be described in chapter 3.5. for comparison.

In the following sections the wide spectral range of ZT refractive index and extinction coefficient will be divided into three parts (as shown in Fig. 4) where different models (Mott-Davis, Wemple-DiDomenico, Drude) will be applied to get more physical insight of ZT films.

3.5. Effect of tin doping on the optical band gap

According to the Mott and Davis [33,34] and Tauc [35] models, the width of the localized states near the mobility edges depends on the degrees of disorder and defects present in the amorphous structure, in particular, differences in coordination number in amorphous state with respect to crystalline state [36,37].

For photon energies ($2.0\,\text{eV} < E < 6.0\,\text{eV}$) short wavelength absorption edge is observed. As mentioned previously, PSEMI oscillator functions are used to model the band edge region, and Lorentz oscillators to model inter band transitions.

For majority of amorphous semiconductors, the optical absorption in the vicinity of the short wavelength absorption edge obeys the Tauc relationship [35]:

$$\alpha E = B \cdot \left(E - E_g^{opt}\right)^2 \quad (3)$$

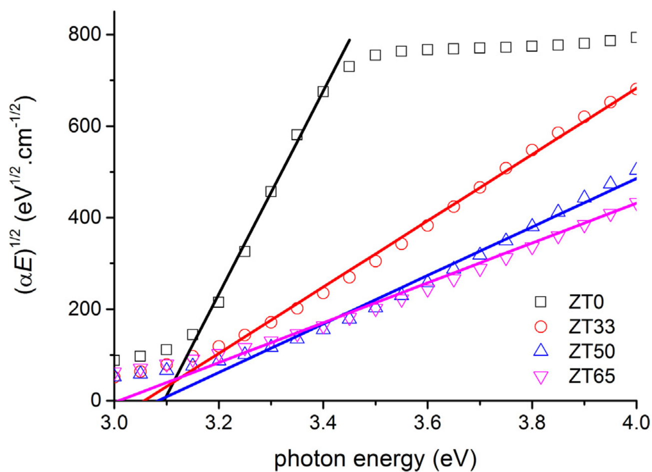

Fig. 5. $(\alpha E)^{1/2}$ as a function of photon energy (symbols) obtained using PSEMI oscillator and its linear part described by Tauc model (solid lines).

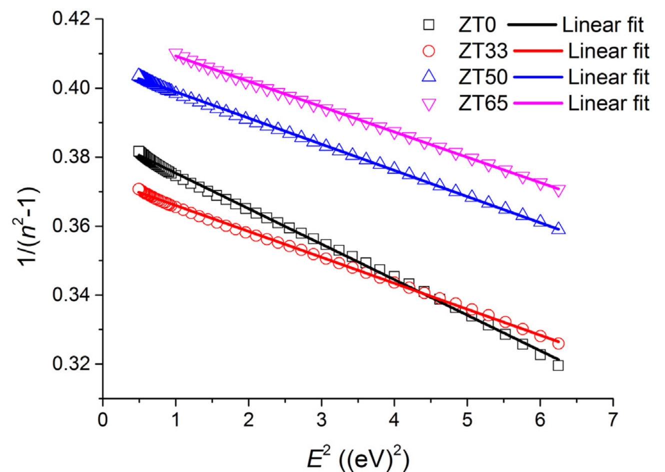

Fig. 6. Dependence of $1/(n^2-1)$ as a function of square photon energy obtained from ellipsometry (symbols) and linear fit of this data (solid lines) according to Wemple-DiDomenico model.

where $\alpha = \frac{4\pi k}{\lambda}$ is absorption coefficient, E is the energy of the incident photon, B is a constant, $E_g{}^{opt}$ is the optical energy gap.

In order to obtain parameters from previous equation dependence in the form of $(\alpha E)^{1/2}$ as a function of photon energy E is depicted at Fig. 5 (left) and the Tauc model (Eq. (3)) is used to describe its linear part (lines). Parameter B can be calculated as $B = \frac{4\pi\sigma_{min}}{nc\Delta E}$ [34], where σ_{min} is the minimum metallic conductivity usually assumed as constant $\approx 350\,\Omega^{-1}\,\text{cm}^{-1}$, n is the refractive index, c is the free space velocity of light and $\Delta E_v = \Delta E$ is the width of localized states near valence band mobility edge can be taken as a measure of a disorder.

The addition of Sn leads to the considerable changes in the sample disorder (the change of parameter $B^{1/2}$). The slope of short wavelength absorption edge (SWAE) decreased from 2218 cm$^{-1/2}$ eV$^{-1/2}$ for the ZT0 to 724, 553 and 435 cm$^{-1/2}$ eV$^{-1/2}$ for the ZT33, ZT50 and ZT65, respectively. The values of the refractive index for 3.0 eV decreased monotonically in the series ZT0, ZT33, ZT50 and ZT65.

Considering that Sn doped samples can be successfully fitted by Tauc-Lorentz oscillator and monotonous decrease of $B^{1/2}$ in the series ZT0, ZT33, ZT50 and ZT65 we can compare the width of localized states near valence band for measured samples as $(\Delta E_{ZTX}/\Delta E_{ZT65}) = (B_{ZT65}/B_{ZTX})/(n_{ZTX}/n_{ZT65})$ using value of refractive index for photon energy close to bandgap energy (≈3.0 eV). For the ZT50 film we obtained $(\Delta E_{ZT50}/\Delta E_{ZT65}) = (435/553)^2/(2.02/1.98) = 0.61$, for the ZT33 film $(\Delta E_{ZT33}/\Delta E_{ZT65}) = (435/724)^2/(2.1/1.98) = 0.34$ and for the ZT0 film we obtained $(\Delta E_{ZT0}/\Delta E_{ZT65}) = (435/2218)^2/(2.15/1.98) = 0.035$ so by Sn doping there was observed pronounced widening of the width of localized states near valence band. All parameters used for this calculation are summarized in Table 2. For comparison values obtained using Tauc-Lorentz model are in Table 2 as well. Although results of precise calculation of ratio of ΔE with values obtained from Tauc-Lorentz model differ, general trend described earlier is the same.

Values of parameter E_g obtained as interception of linear part of dependence of $(\alpha E)^{1/2}$ as a function of photon energy E with the energy axis are summarized in Table 2 as well and compared with the parameter E_g obtained from the Tauc-Lorentz model [31,32]. As can be seen from Table 2 in our case the value of E_g does not change significantly during Sn doping. As was mentioned earlier Tauc-Lorentz oscillator is enable to describe short wavelength absorption edge for ZT0 sample.

It has been previously reported for chemical vapor deposited ZnO that as the growth temperature is reduced from 500 to 200 °C, the films become more amorphous, and the extended localization in the conduction and valence bands increases [38]. Likewise, since the incorporation of tin induces an amorphous phase in ZnO, one can expect the increase in local disorder with Sn doping, resulting in the increase of ΔE as demonstrated here.

3.6. Effect of tin doping on the refractive index dispersion data

The effect of tin doping on the refractive index dispersion data in the semi-transparent part of spectra below the bandgap ($0.5 < E < 2.5$ eV) is further investigated using a Wemple-DiDomenico model [39,40]. The refractive index data can be fitted in this spectral range to the single oscillator expression

$$n^2(E) = 1 + \frac{E_0 \cdot E_d}{E_0^2 - E^2} \tag{4}$$

where E is the photon energy, E_0 is the energy of the effective dispersion oscillator and E_d is the dispersion energy. From linear regression of dependence $\left(n^2 - 1\right)^{-1}$ against E^2 (as shown in Fig. 6), the parameters E_d and E_0 could be calculated.

The parameter E_d, which is a measure of the intensity of the inter-band optical transition, is related to other physical parameters of the material through the following empirical relationship [39,40],

$$E_d(eV) = \beta \cdot N_c \cdot N_e \cdot Z_a \tag{5}$$

where N_c is the effective coordination number of the cation nearest-neighbor to the anion, Z_a is the formal chemical valence of the anion, N_e is the effective number of valence electrons per anion and β is a two valued constant with either an ionic or covalent value ($\beta_{ionic} = 0.26 \pm 0.03$ eV and $\beta_{covalent} = 0.37 \pm 0.04$ eV).

Fig. 7 shows the variation of E_d and E_0 as a function of tin doping of the ZT films. E_d is ~16 eV in undoped ZT0 and ~18 eV in the doped ZT films. Given that ZT0 is a polycrystalline structure whereas doped ZT films are amorphous, the E_d values are very similar. A similar small variation of E_d values has been reported for crystalline SiO_2 and amorphous fused silica, indicating that E_d is not affected by the loss of long range order [39]. Our E_d value of ZT0 (16 eV) is also very similar to that reported by Wemple (17.1 eV). There is no significant difference in E_d values between the doped ZT films (ZT33, 50 and 65). In spite of Eq. (5) increase of E_d between undoped ZT0 and Sn doped ZT33, ZT50 and ZT65 could be explained both by increase of β and by increase of N_e. It is reasonable to suppose creation of Sn-O bonds instead of Zn-O bonds, with the

Please cite this article in press as: P. Janicek, et al., Spectroscopic ellipsometry characterization of ZnO:Sn thin films with various Sn composition deposited by remote-plasma reactive sputtering, Appl. Surf. Sci. (2016), http://dx.doi.org/10.1016/j.apsusc.2016.10.169

Table 2
$B^{1/2}$ = Slope of linear part of the dependence of $(\alpha E)^{1/2}$ as a function of photon energy E obtained using PSEMI oscillator or Tauc-Lorentz oscillator, n (3.0 eV) = refractive index for 3.0 eV and parameter E_g obtained using PSEMI oscillator or Tauc-Lorentz oscillator.

Sample	$B^{1/2}{}_{PSEMI}$ ($cm^{-1/2}$ $eV^{-1/2}$)	$E_g{}^{PSEMI}$ (eV)	n (3.0 eV)	$B^{1/2}{}_{TL}$ ($cm^{-1/2}$ $eV^{-1/2}$)	$E_g{}^{TL}$ (eV)
ZT0	2218	3.1	2.15	–	–
ZT33	724	3.06	2.10	575	3.05
ZT50	553	3.08	2.02	500	3.06
ZT65	435	3.0	1.98	431	3.0

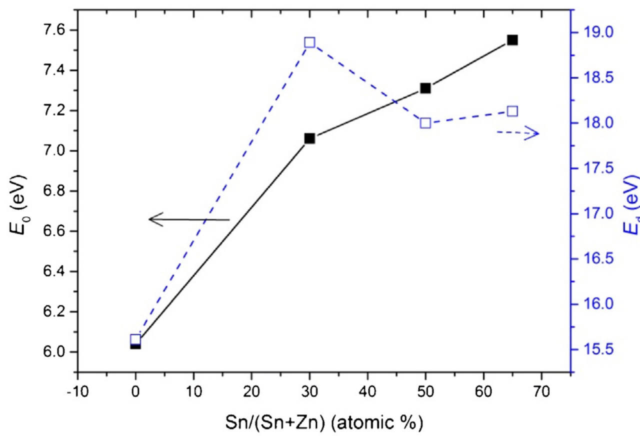

Fig. 7. Parameters E_d and E_0 as a function of Sn content.

former being more covalent therefore increasing β. The value of E_d obtained in our study is close to the E_d ~14 eV reported for AZO produced by direct current reactive magnetron sputtering [13], with a small variation in the E_d with varying substrate temperatures.

E_0 is ~6 eV in undoped ZT0 and ~7 eV in the doped ZT films. Our E_0 value of ZT0 is again very similar to that reported by Wemple (6.4 eV) [40]. A small increase in E_0 is observed as tin doping increases from ZT33 to ZT65. Parameter E_0 is associated with distance of centroids of the valence and conduction bands and therefore with optical bandgap $\left(E_0 \approx 1.5 + 1.25E_g^{opt}\right)$ [41,42]. Such increase in E_0 with doping has also been reported in AZO [13] and in IZO [11].

3.7. Effect of tin doping on the free carrier absorption

In NIR-MIR part of spectra, free carrier absorption and the long wavelength absorption edge are present. These two contributions can be separated.

When focusing on NIR part of spectra ($0.2 < E < 0.5$ eV, $1000 < \lambda < 4000$ nm) a Drude-only model could be used with MSE less than 6 to investigate the effect of tin doping on the free carrier absorption [21]. As shown in Fig. 8 (left), the increase of extinction coefficient with increasing tin content in the NIR part of spectra is observed and is typically correlated with increase of electric conductivity.

The model dielectric function described by Drude model is expressed by [20],

$$\tilde{\varepsilon}_{Drude} = \frac{-\left(h/(2\pi)\right)^2}{\varepsilon_0 \rho \left(\tau E^2 + i\left(h/(2\pi)\right)E\right)} \tag{6}$$

where h is the Planck constant, and ε_0 is the permittivity of free space. From the Drude model, resistivity, ρ, and mean scattering time, τ, as free parameters could be extracted. Another two parameters, free carrier concentration, N, and carrier mobility, μ, could be calculated using effective mass m^* and the carrier charge e

$$\rho = \frac{m^*}{Ne^2\tau} = \frac{1}{e\mu N} \tag{7}$$

Free carrier concentration and mobility could be further derived using $m^* = 0.34 \times m_0$ [43] and the results are depicted in Fig. 8 (right). With increasing Sn doping free carrier concentration is increasing from 4.4×10^{18} cm^{-3} for ZT33 to 7.6×10^{18} cm^{-3} for ZT65 with mobilities in the range of 6–16 cm^2/Vs. Although values of free carrier concentration and mobility cannot be confirmed experimentally by Hall measurement due to the fact that films are highly resistive, these values are comparable with previous study of Islam et al. [44]. The decrease in mobility with increasing carrier concentration is typically attributed to scattering due to ionized impurities [45].

4. Conclusions

Spectroscopic ellipsometry study was conducted on the ZnO:Sn with various tin doping produced by remote-plasma reactive sput-

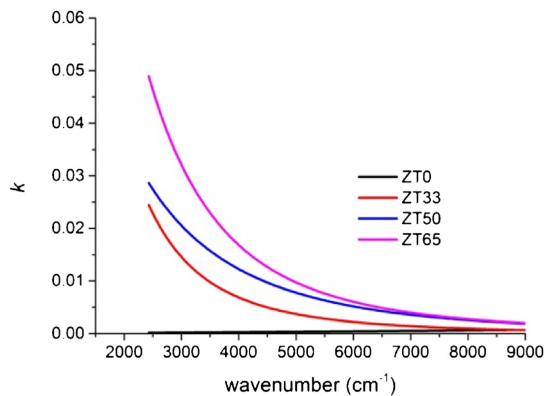

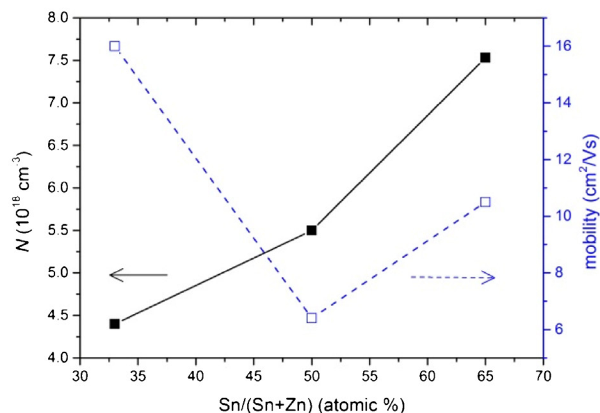

Fig. 8. Calculated extinction coefficient k for Drude-only model, as a function of wavenumber in the MIR part of spectra (left). Calculated free carrier concentration N and mobility μ as a function of Sn content (right).

Please cite this article in press as: P. Janicek, et al., Spectroscopic ellipsometry characterization of ZnO:Sn thin films with various Sn composition deposited by remote-plasma reactive sputtering, Appl. Surf. Sci. (2016), http://dx.doi.org/10.1016/j.apsusc.2016.10.169

tering. While undoped ZnO is polycrystaline, doped ZnO:Sn films are amorphous [14]. The refractive index and extinction coefficient of those films over the broad spectral range of the MIR-VIS-UV region ($0.05 < E < 6.0$ eV) were obtained by the best fit of ellipsometry data parametrizing ZnO:Sn model dielectric function by a PSEMI oscillator for description of short wavelength absorption edge, a Drude oscillator for description of free carrier absorption in NIR part of spectra (not used in the case of ZT0 sample) and Lorentz oscillators for the long wavelength absorption edge and intra-band absorption in the UV part of the spectra.

Using a Mott-Davis model in the vicinity of the absorption edge ($3.0 < E < 4.0$ eV), the width of the localized states is significantly increased by Sn doping indicating the increase of local disorder with tin doping. Using Wemple-DiDomenico single oscillator dispersion in the semi-transparent spectrum ($0.5 < E < 2.5$ eV), the intensity of interband optical transition, E_d, shows an increase ~2 eV from undoped ZT0 to doped ZT films probably due to increase of number of Sn-O bonds which are more covalent that Zn-O bonds and there is no obvious difference between the doped ZT films. The energy of the effective dispersion oscillator (E_0) increase with increasing tin doping indicating distancing of centroids of the valence and conduction bands. Using a Drude-only model in the NIR part of spectra ($0.2 < E < 0.5$ eV, $1000 < \lambda < 4000$ nm), the free carrier concentration increases with tin doping from 4.4×10^{18} cm^{-3} for ZT33 to 7.6×10^{18} cm^{-3} for ZT65, and mobilities in the range of 6–16 cm^2/Vs were calculated. These results are comparable with other studies e.g. [45].

The range of transparency, i.e. value of parameter E_g, of prepared ZnO:Sn layers is not dramatically affected by tin doping whereas electrical conductivity could be controlled by tin doping. The value of refractive index, ~2 obtained for doped ZT samples, are similar to that reported for a-IGZO. These results indicate possibility of utilization of prepared layers as an indium free substitution of a-IGZO.

Acknowledgements

Authors appreciate financial support from the grant CZ.1.05/4.1.00/11.0251 from the Ministry of Education, Youth and Sports of the Czech Republic as well as financial support from the grant No. EP/M013650/1 from Engineering and Physical Sciences Research Council UK.

Authors would like to acknowledge Prof. L. Tichy from Joint Laboratory of Solid State Chemistry of the Institute of Macromolecular Chemistry of AS CR and University of Pardubice for valuable comments, suggestions and discussion.

References

[1] T. Minami, Present status of transparent conducting oxide thin-film development for Indium-Tin-Oxide (ITO) substitutes, Thin Solid Films 516 (2008) 5822–5828.
[2] D.R. Sahu, S.-Y. Lin, J.-L. Huang, ZnO/Ag/ZnO multilayer films for the application of a very low resistance transparent electrode, Appl. Surf. Sci. 252 (2006) 7509–7514.
[3] K. Postava, H. Sueki, M. Aoyama, T. Yamaguchi, C. Ino, Y. Igasaki, M. Horie, Spectroscopic ellipsometry of epitaxial ZnO layer on sapphire substrate, J. Appl. Phys. 87 (2000) 7820–7824.
[4] K. Postava, H. Sueki, M. Aoyama, T. Yamaguchi, K. Murakami, Y. Igasaki, Doping effects on optical preperties of epitaxial ZnO layers determined by spectroscopic ellipsometry, Appl. Surf. Sci. 175–176 (2001) 543–548.
[5] X.W. Sun, H.S. Kwok, Optical properties of epitaxially grown zinc oxide films on sapphire by pulsed laser deposition, J. Appl. Phys. 86 (1999) 408–411.
[6] E. Mammadov, N. Naghavi, Z. Jehl, G. Renou, T. Tiwald, N. Mamedov, D. Lincot, J.F. Guillemoles, Dielectric function of zinc oxide thin films in a broad spectral range, Thin Solid Films 571 (2014) 593–596.
[7] E. Fortunato, P. Barquinha, R. Martins, Oxide semiconductor thin-film transistors: a review of recent advances, Adv. Mater. 24 (2012) 2945–2986.
[8] J.K. Jeong, The status and perspectives of metal oxide thin-film transistors for active matrix flexible displays, Semicond. Sci. Technol. 26 (2011) 034008.
[9] H.Q. Chiang, J.F. Wager, R.L. Hoffman, J. Jeong, D.A. Keszler, High mobility transparent thin-film transistors with amorphous zinc tin oxide channel layer, Appl. Phys. Lett. 86 (2005) 013503.
[10] T. Kamiya, K. Nomura, H. Hosono, Electronic structure of the amorphous oxide semiconductor a-InGaZnO4-x: Tauc-Lorentz optical model and origins of subgap states, Phys. Status Solidi (a) 206 (2009) 860–867.
[11] A.C. Galca, G. Socol, V. Craciun, Optical properties of amorphous-like indium zinc oxide and indium gallium zinc oxide thin films, Thin Solid Films 520 (2012) 4722–4725.
[12] C. Talagrand, X. Boddaert, D.G. Selmeczi, C. Defranoux, P. Collot, Ellipsometry study of process deposition of amorphous indium gallium zinc oxide sputtered thin films, Thin Solid Films 590 (2015) 134–140.
[13] X. Gao, Y. Liang, Q.-G. Lin, Analysis of the optical constants of aluminum-doped zinc-oxide films by using the single-oscillator model, J. Korean Phys. Soc. 57 (2010) 710–714.
[14] K.M. Niang, J. Cho, S. Heffernan, W.I. Milne, A.J. Flewitt, Optimisation of amorphous zinc tin oxide thin film transistors by remote-plasma reactive sputtering, J. Appl. Phys. 120 (2016) 085312.
[15] C.M. Herzinger, B. Johs, W.A. McGahan, J.A. Woollam, W. Paulson, Ellipsometric determination of optical constants for silicon and thermally grown silicon dioxide via a multi-sample multi-wavelength, multi-angle investigation, J. Appl. Phys. 83 (1998) 3323–3336.
[16] Y.C. Liu, J.H. Hsieh, S.K. Tung, Extraction of optical constants of zinc oxide thin films by ellipsometry with various models, Thin Solid Films 510 (2006) 32–38.
[17] Guide to using WVASE32 Software for Spectroscopic Ellipsometry Data Acquisition and Analysis, in, J. A. Woollam Co. Inc., 2000.
[18] Y.S. Ihn, T.J. Kim, T.H. Ghong, Y.D. Kim, D.E. Aspnes, J. Kossut, Parametric modeling of the dielectric functions of Cd1-xMgxTe alloy films, Thin Solid Films 455 (2004) 222–227.
[19] B. Johs, C.M. Herzinger, J.H. Dinan, A. Cornfeld, J.D. Benson, Development of a parametric optical constant model for Hg1-xCdxTe for control of composition by spectroscopic ellipsometry during MBE growth, Thin Solid Films 313 (1998) 137–142.
[20] F. Wooten, Optical Properties of Solids, Academic Press, New York, 1972.
[21] T.E. Tiwald, D.W. Thompson, J.A. Woollam, W. Paulson, R. Hance, Thin Solid Films 313 (1998) 661–666.
[22] D.A.G. Bruggeman, Berechnung verschiedener physikalischer Konstanten von heterogenen Substanzen. I. Dielektrizitätskonstanten und Leitfähigkeiten der Mischkörper aus isotropen Substanzen, Ann. Phys. (Leipzig) 24 (636) (1935) 636–664.
[23] H. Fujiwara, M. Kondo, A. Matsuda, Real-time spectroscopic ellipsometry studies of the nucleation and grain growth processes in microcrystalline silicon thin films, Phys. Rev. B 63 (2001) 115306.
[24] J. Koh, Y. Lu, C.R. Wronski, Y. Kuang, R.W. Collins, T.T. Tsong, Y.E. Strausser, Correlation of real time spectroellipsometry and atomic force microscopy measurements of surface roughness on amorphous semiconductor thin films, Appl. Phys. Lett. 69 (1996) 1297–1299.
[25] D. Franta, I. Ohlídal, P. Klapetek, P. Pokorný, Characterization of the boundaries of thin films of TiO2by atomic force microscopy and optical methods, Surf. Interface Anal. 34 (2002) 759–762.
[26] Q.H. Li, D. Zhu, W. Liu, Y. Liu, X.C. Ma, Optical properties of Al-doped ZnO thin films by ellipsometry, Appl. Surf. Sci. 254 (2008) 2922–2926.
[27] S.W. Xue, X.T. Zu, W.G. Zheng, H.X. Deng, X. Xiang, Effects of Al doping concentration on optical parameters of ZnO:Al thin films by sol-gel technique, Phys. B Condens. Matter 381 (2006) 209–213.
[28] H. Kim, A. Piqué, J.S. Horwitz, H. Murata, Z.H. Kafafi, C.M. Gilmore, D.B. Chrisey, Effect of aluminum doping on zinc oxide thin films grown by pulsed laser deposition for organic light-emitting devices, Thin Solid Films 377–378 (2000) 798–802.
[29] N. Ashkenov, B.N. Mbenkum, C. Bundesmann, V. Riede, M. Lorenz, D. Spemann, E.M. Kaidashev, A. Kasic, M. Schubert, M. Grundmann, G. Wagner, H. Neumann, V. Darakchieva, H. Arwin, B. Monemar, Infrared dielectric functions and phonon modes of high-quality ZnO films, J. Appl. Phys. 93 (2003) 126–133.
[30] P. Barquinha, L. Pereira, G. Goncalves, R. Martins, E. Fortunato, Toward high-performance amorphous GIZO TFTs, J. Electrochem. Soc. 156 (2009) H161–H168.
[31] G.E. Jellison Jr., F.A. Modine, Parametrization of the optical functions of amorphous materials in the interband region, Appl. Phys. Lett. 69 (1996) 371–374.
[32] G.E. Jellison Jr., F.A. Modine, Parametrization of the optical functions of amorphous materials in the interband region erratum, Appl. Phys. Lett. 69 (1996) 2137–2139.
[33] N.F. Mott, E.A. Davis, Electronic Processes in Non-Crystalline Materials, Clarendon Press, Oxford, 1979.
[34] E.A. Davis, N.F. Mott, Conduction in non-crystalline systems V. Conductivity, optical absorption and photoconductivity in amorphous semiconductors, Philos. Mag. 22 (1970) 0903–0922.
[35] J. Tauc, in: J. Tauc (Ed.), Amorphous and Liquid Semiconductors, Plenum Press, New York, 1974.
[36] S.R. Ovshinsky, D. Adler, Local structure, bonding, and electronic properties of covalent amorphous semiconductors, Contemp. Phys. 19 (2006) 109–126.
[37] M.L. Theye, Proceeding of the Fifth International Conference on Amorphous and Liquid Semiconductors, Garmisch-Partenkirchen, 1973.

[38] S.T. Tan, B.J. Chen, X.W. Sun, W.J. Fan, H.S. Kwok, X.H. Zhang, S.J. Chu, Blueshift of optical band gap in ZnO thin films grown by metal-organic chemical-vapor deposition, J. Appl. Phys. 98 (2005) 013505.
[39] S.H. Wemple, Refractive-index behavior of amorphous semiconductors and glasses, Phys. Rev. B 7 (1973) 3767–3777.
[40] S.H. Wemple, M. DiDomenico, Behavior of the electronic dielectric constant in covalent and ionic materials, Phys. Rev. B 3 (1971) 1338–1351.
[41] K. Tanaka, Optical properties and photoinduced changes in amorphous As-S films, Thin Solid Films 66 (1980) 271–279.
[42] H. Ticha, L. Tichy, Semiempirical relation between non-linear susceptibility (refractive index), linear refractive index and optical gap and its application to amorphous chalcogenides, J. Optoelectron. Adv. Mater. 4 (2002) 381–386.
[43] H. Morkoç, U. Ozgur, Zinc Oxide, Wiley-VCH, 2009, pp. 1–76.
[44] M.A. Islam, K.S. Rahman, F. Haque, N.A. Khan, M. Akhtaruzzaman, M.M. Alam, H. Ruslan, K. Sopian, N. Amin, Effect of Sn doping on the properties of nano-structured ZnO thin films deposited by co-sputtering technique, J. Nanosci. Nanotechnol. (2015) 9184–9191.
[45] R. Martins, P. Barquinha, A. Pimentel, L. Pereira, E. Fortunato, Transport in high mobility amorphous wide band gap indium zinc oxide films, Phys. Stat. Sol. (a) 202 (2005) R95–R97.

Please cite this article in press as: P. Janicek, et al., Spectroscopic ellipsometry characterization of ZnO:Sn thin films with various Sn composition deposited by remote-plasma reactive sputtering, Appl. Surf. Sci. (2016), http://dx.doi.org/10.1016/j.apsusc.2016.10.169